Size dependent lattice constant change of thiol self-assembled monolayer modified Au nanoclusters studied by grazing incidence x-ray diffraction

Toshihiro Kondo[a,b], *Takuya Masuda*[a], *Motoko Harada*[c], *Osami Sakata*[d], *Yoshio Katsuya*[d], *and Kohei Uosaki*[a,c,e,*]

[a]Grobal Research Center for Environmental and Energy Based on Nanomaterials Science (GREEN), National Institute for Materials Science (NIMS), Tsukuba 305-0044, Japan

[b]Graduate School of Humanities and Sciences, Ochanomizu University, Tokyo 112-8610, Japan

[c]Division of Chemistry, Graduate School of Science, Hokkaido University, Sapporo 060-0810, Japan

[d]Synchrotron X-ray Station at SPring-8, Research Network and Facility Service Division, National Institute for Materials Science (NIMS), Hyogo 679-5148, Japan

[e]International Center for Materials Nanoarchitectonics (MANA), National Institute for Materials Science (NIMS), Tsukuba 305-0044, Japan

[*]Corresponding Author. Tel.: +81-29-860-4301; fax: +81-29-851-3362. E-mail address: UOSAKI.kohei@nims.go.jp

ABSTRACT

Size and lattice constant of thiol self-assembled monolayer (SAM)-modified gold nanoclusters (GNCs) assembled on Au(111) surfaces after each electrochemical treatment were investigated using grazing incidence x-ray diffraction (GIXRD). When the potential was swept between 0 and 1.3 V (vs. Ag/AgCl), the size and lattice constant of GNCs slightly decreased due to the oxidative desorption of the SAMs. As the number of potential cycles increased, the size of GNCs started to increase due to the aggregation, while the lattice constant continued to decrease due to further desorption of the SAMs from the GNCs. After most of the SAMs were removed from the GNCs, the size and lattice constant monotonically increased with the number of potential cycles. The size dependent lattice constant change was observed when GNCs were smaller than ~35Å.

KEYWORDS: Gold nanoclusters (GNCs), Size dependence of lattice constant of GNCs, Grazing incidence x-ray diffraction (GIXRD), Self-assembled monolayer (SAM)

1. Introduction

It is very important to clarify the relationship between the size and interatomic layer distance, i.e., lattice constant, of nanoclusters, since these structural parameters are critical factors determining the physical and chemical properties of nanoclusters, such as catalytic activity. Both theoretical predictions [1-6] and experimental results [6-14] have indicated that lattice constant of small metallic nanoclusters is smaller than that of the corresponding bulk crystals. However, the systematic study on the size dependent lattice constant change of metal nanoclusters has yet to be carried out because of the difficulty in precise control of the cluster size.

Previously, we succeeded [16-24] to synthesize gold nanoclusters (GNCs), of which surface was covered with the mixed self-assembled monolayers (SAMs) of mercaptoundecanoic acid (MUA),

hexanethiol (C_6SH), and ferrocenylhexanethiol (FcC_6SH), using the methods by Brust et al. [25] and Hostetler et al. [26] and to construct the multilayers of GNCs on the solid surface, using the cation/anion electrostatic interaction [27-31]. When the potential was made more positive than that for the oxidative decomposition of the thiol SAM on gold [32-35], the SAM was gradually removed from the GNCs and GNCs started to aggregate [22,23].

In this study, the size and lattice constant of GNCs were monitored using grazing incidence x-ray diffraction (GIXRD) after each electrochemical treatment, i.e., potential cycles between 0 and 1.30 V (vs. Ag/AgCl), where the thiol SAM is oxidatively decomposed. In the initial stage, the size and lattice constant of GNCs decreased from ca. 16 Å to ca. 12 Å and from ca. 4.19 Å to ca. 4.01 Å, respectively, due to the oxidative decomposition of the SAMs. Then, the size of GNCs increased to ca. 17 Å with the number of cycles due to the aggregation, while the lattice constant continued to decrease to ca. 3.93 Å due to further desorption of the SAMs. After most of the SAMs were removed from the GNCs, the size and lattice constant monotonically increased to ca. 40 Å and ca. 4.08 Å, respectively, proving the size dependent lattice constant change of GNCs during the aggregation. When the size of GNCs was larger than ~35 Å, the lattice constant became almost constant at around 4.08 Å which is identical to that of bulk gold.

2. Experimental

GNCs modified with the mixed SAMs of MUA, C_6SH, and FcC_6SH were prepared by the methods previously reported [16-19,21]. Multilayers of GNCs were prepared on a commercially available Au(111) substrate, which was annealed and quenched prior to use, by repeating the two-step dip and rinse cycles for 10 times based on the carboxylate/poly(allylamine hydrochloride) (PAH)/carboxylate electrostatic interaction [16-19,21-23]. Cyclic voltammograms (CVs) of the Au(111) electrode modified with these mixed SAM modified GNCs multilayers were measured in a deaerated 0.1 M $HClO_4$ solution at a scan rate of 50 mV s^{-1} in the potential range between 0 and 1.30 V with respect to the Ag/AgCl electrode. The samples before and after a certain number of potential cycles were set on a six-circle

diffractomator installed in an undulator-magnet beamline BL15XU at SPring-8 and GIXRD measurements were carried out in air with an x-ray energy of 11.5 keV and an incident angle of 0.2°. It was confirmed that x-ray irradiation during the GIXRD measurement did not cause any damage to the sample, from the fact that no significant change was observed in the CVs after the GIXRD measurements. GIXRD profiles were fitted by summation of two Lorentzian functions to obtain the peak positions and fwhm (full width of half maximum).

3. Results and Discussion

Figure 1 shows CVs of the Au(111) electrode modified with GNC/PAH layers, measured in the 0.1 M $HClO_4$ solution. The CVs are almost the same as our previous reports [22,23]. Redox waves due to the redox of the ferrocene/ferrocenium couple (Fc/Fc^+) observed at around 0.35 V gradually decreased by repeating the potential cycles between 0 and 1.30 V, confirming the oxidative decomposition of the thiol SAMs. Simultaneously, oxidation and reduction current due to the formation and reduction of Au oxide at around 1.2 V and 0.9 V, respectively, increased with the number of potential cycles.

Figure 2 shows typical GIXRD profiles of the samples before and after several potential cycles. Before the potential cycles, a broad peak composed of two components due to the Bragg reflections of Au(111) and Au(200) around 2θ of 26.5° and 30.6° [36-40], respectively, was observed. It should be noted that the (111) reflection peaks were not from the Au(111) substrate but from GNCs because the measurements were carried out in an in-plane configuration. Azimuthal angle was fixed to avoid surface x-ray diffraction from the Au(111) substrate, such as <110> and <112>. As clearly seen in the profiles, these peaks became sharper as increase in the number of the potential cycles.

The size and interatomic layer distance of GNCs can be obtained by Scherrer's and Bragg's equations, respectively, as follows [41-46]:

$$D = (K \times \lambda) / (\beta \times \cos \theta) \quad (1)$$

$$d = \lambda / (2 \times \sin \theta) \quad (2)$$

where D (Å), K, λ (Å), β (rad), θ (degree), and d (Å) are an average size of GNCs, Scherrer's constant (0.9 used in this study as assuming to be a spherical shape), wavelength of x-ray (1.078 Å), fwhm, half of diffraction angle, and layer distance, respectively. Lattice constants were obtained from interatomic layer distances of the (111) and (200) reflections.

Figure 3 shows the cluster size and lattice constant as a function of the number of potential cycles, together with reductive charge densities for Fc/Fc^+ and Au oxide. The cluster size and lattice constant obtained from fwhm and 2θ of the (111) reflection (blue points in Fig. 3(a)) were almost the same as those obtained from the (200) reflection (red points in Fig. 3(a)), suggesting that the peak fitting in the present study is reasonable.

Before the potential cycles, i.e., GNCs were fully covered by the thiol SAMs, the cluster size was ca. 16 Å, which is in reasonable agreement with that (ca. 18 Å) previously obtained from TEM image [18,19]. Lattice constant obtained from the interatomic layer distances of the (111) reflection was ca. 4.19 Å, which were somewhat larger than that of bulk gold, 4.08 Å. This result shows that the thiol SAMs strongly adsorbed on the GNCs surface, leading to the expansion of the interatomic layer distance of GNCs. The cycle number dependences of the size and lattice constant of GNCs can be divided into four steps: As increase in the number of the potential cycles, (step (i)) the size and lattice constant decreased to ca. 12 Å (Fig. 3 (a)) and ca. 4.01 Å (Fig. 3 (b)), respectively, up to 2nd cycle. In this step, the charge density for Fc/Fc^+ decreased (Fig. 3(c)), showing that a small amount of the thiol SAMs including FcC_6SH was oxidatively decomposed and removed from the GNCs surface. As a result, part of the GNCs surface was exposed to the electrolyte solution, leading to increase in the charge density for the reduction of Au oxide (Fig. 3(c)). When the strongly adsorbed SAMs are desorbed from the GNCs, interatomic layer distance of GNCs can be shortened. In addition, part of gold atoms bound to the sulfur atoms can be removed together with the SAMs, leading to the contraction of GNCs. (step (ii)) Oxidative decomposition of the SAMs further proceeded and the FcC_6SH SAMs were totally removed up to 12th cycle (Fig. 3 (c)). Accordingly, the charge density for the reduction of Au oxide increased due to the stripping of the SAMs as well as in the case of step (i) (Fig. 3(c)). The size of

GNCs gradually increased to ca. 17 Å with the number of cycles due to the aggregation of GNCs (Fig. 3 (a)), while the lattice constant first decreased up to 8th cycle to ca. 3.93 Å due to further desorption of SAMs including fragments with sulfur atoms from the GNCs and then started to increase from 8th cycle. In this step, desorption of the SAMs and aggregation of GNCs simultaneously take place. Since decrease of the lattice constant was attributed to the desorption of the SAMs, increase of the lattice constant from 8th cycle can be considered to be due to the aggregation of GNCs. According to the charge density for Fc/Fc^+ (Fig. 3(c)), more than 70% of FcC_6SH in the mixed SAMs were already removed from the surface after 8th cycle, suggesting that increase of the lattice constant due to the aggregation became more dominant at this stage. (step (iii)) After most of the SAMs were removed, the size and lattice constant of GNCs monotonically increased to ca. 35 Å (Fig. 3 (a)) and 4.07 Å (Fig. 3 (b)), respectively, showing the aggregation of "bare" GNCs. The charge density for the reduction of Au oxide still increased although that for Fc/Fc^+ became zero at 12th cycle, suggesting that the SAMs without ferrocene moieties and other fragments with sulfur atoms were remained on the GNC surface in this step. Finally, (step (iv)) GNCs gradually grew to ca. 40 Å (Fig. 3 (a)) up to 50th cycle while the lattice constant remained almost the same around ca. 4.08 Å (Fig. 3 (b)), which is identical to that of the bulk gold. Thus, it was experimentally demonstrated that the lattice constant depends on the size of GNCs when GNCs were smaller than ~35 Å. The charge density for the reduction of Au oxide increased up to 30th cycle and then gradually decreased from 30th cycle to 50th cycle (Fig. 3(c)), This indicates that all the SAMs including the fragments were completely removed from the surface after 30th cycle but the electrochemical-active area of GNCs still decreased up to 50th cycle due to the aggregation.

The relationship between size and lattice constant of GNCs were previously discussed by Page et al. [47] and Harada et al [48]. The authors both concluded that the lattice constant of GNCs was independent of the size, probably because they used GNCs larger than 40 Å. This is indeed consistent with our observation that the lattice constant became almost constant when GNCs were larger than ~35 Å. For other metal nanoclusters such as copper [7,8] and nickel [7] with a size of 10 - 50 Å, it was reported that lattice constant became smaller with decreasing cluster size. A major reason for the size

dependent lattice constant change was proposed to be an increase of bond energy as a result from an increase in the number of surface atoms [7,8]. Such contraction of the lattice constant of copper nanoclusters was theoretically supported using the embedded atom method based on the density functional theory [1].

4. Conclusion

Size dependent lattice constant change of the SAM-modified GNCs, assembled on the Au(111) surface was systematically investigated using GIXRD in combination with electrochemical treatments. Size and lattice constant of GNCs decreased from 16 Å to 12 Å and from 4.19 Å to 4.01 Å, respectively, due to the oxidative decomposition of the SAMs. Along with further oxidative decomposition, the lattice constant decreased to 3.93 Å, while GNCs started to aggregate to form larger clusters. After most of the SAMs were removed from the GNCs, the size and lattice constant monotonically increased to 35 Å and 4.07 Å, respectively, due to the aggregation of “bare” GNCs. Although GNCs gradually grew up to 40 Å with the number of potential cycles, the lattice constant was remained almost constant, 4.08 Å, which is the same as that of bulk gold.

ACKNOWLEDGMENTS

This work was partially supported by Grant-in-Aid for Scientific Research C (KAKENHI, No. 26410008) from Ministry of Education, Culture, Sports, Science, and Technology. TK acknowledges an open-lab program at the Global Research Center for Environment and Energy based on Nanomaterials Science (GREEN) in National Institute for Materials Science (NIMS). The synchrotron radiation experiments were performed as projects by the Japan Synchrotron Radiation Research Institute (JAERI) (proposal Nos. 2011B4506, 2012A4504, and 2012B4503).

FIGURE CAPTIONS

Figure 1 CVs of the Au(111) electrode modified with the GNC/PAH layers, measured in a deaerated 0.1 M $HClO_4$ solution with a scan rate of 50 mV s^{-1}. Number of cycles is shown in the figure.

Figure 2 Typical GIXRD profiles of the Au(111) electrode modified with the GNC/PAH layers (a) before and after the potential cycles (b) 1, (c) 8, and (d) 30 times. Black dots: experimental data. Red, blue, and black lines: fitting curves of the (111) reflection, the (200) reflection, and their summation, respectively.

Figure 3 (a) Cluster sizes calculated from fwhm of (111) (blue) and (200) (red) reflections, (b) lattice constants calculated from 2θ of (111) (blue) and (200) (red) reflections, and (c) charge densities calculated from the reductive peaks of ferrocene/ferrocenium couple (blue) and gold oxide (red), as a function of number of the potential cycles.

REFERENCES

[1] M. Katagiri, A. Miyamoto, T. R. Coley, Y. S. Li, J. M. Newsam, Deposition and surface dynamic of metals studied by the embedded-atom molecular dynamics method, Mol. Simul. 17, (1996), 1-19.

[2] M. B. Gordon, F. Cyrot-Lackmann, M. C. Desjonqueres, Relaxation and Stability of Small Transition-Metal Particles, Surf. Sci. 80, (1979), 159-164.

[3] D. Tomanek, S. Mukherjee, K. H. Bennemann, Simple Theory for the Electronic and Atomic-Structure of Small Clusters, Phys. Rev. B 28, (1983), 665-673.

[4] H. Li, P. D. Han, X. B. Zhang, M. Li, Size-dependent melting point of nanoparticles based on bond number calculation, Mater. Chem. Phys. 137, (2013), 1007-1011.

[5] W. G. Wolfer, Elastic properties of surfaces on nanoparticles, Acta Materialia 59, (2011), 7736-7743.

[6] A. Janz, A. Köckritz, L. Yao, A. Martin, Fundamental Calculations on the Surface Area Determination of Supproted Gold Nanoparticles by Alkanethiol Adsorption, Langmuir 26, (2010), 6783-6789.

[7] G. Apai, J. F. Hamilton, J. Stohr, A. Thompson, Extended X-Ray-Absorption Fine-Structure of Small Cu and Ni Clusters - Binding-Energy and Bond-Length Changes with Cluster Size, Phys. Rev. Lett. 43, (1979), 165-169.

[8] P. A. Montano, G. K. Shenoy, E. E. Alp, W. Schulze, J. Urban, Structure of Copper Microclusters Isolated in Solid Argon, Phys. Rev. Lett. 56, (1986), 2076-2079.

[9] K. Tamura, H. Oyanagi, T. Kondo, M. Koinuma, K. Uosaki, Structural study of electrochemically deposited Cu on p-GaAs(100) in H_2SO_4 solution by in situ surface-sensitive X-ray absorption fine structure measurements, J. Phys. Chem. B 104, (2000), 9017-9024.

[10] D. Zanchet, H. Tolentino, M. C. Martin Alves, O. L. Alves, D. Ugarte, Inter-atomic distance contraction in thiol-passivated gold nanoparticles, Chem. Phys. Lett. 323, (2000), 167-172.

[11] S. B. Erenburg, B. L. Moroz, N. V. Bausk, V. I. Bukhtiyarov, S. Nikitenko, XAS study on microstructure of Au nanoparticles deposited onto alumina, Nuclear Instr. Methods Phys. Res. A 575, (2007), 105-108.

[12] W. Vogel, Size Contraction in Pt/C and PtRu/C Commersial E-TEK Electrocatalysts: An in Situ X-ray Diffraction Study, J. Phys. Chem. C 112, (2008), 13475-13482.

[13] H. Ikemoto, A. Goyo, T. Miyanaga, Size Dependence of the Local Structure and Atomic Correlations in Tellurium Nanoparticles, J. Phys. Chem. C 115, (2011), 2931-2937.

[14] Y. Y. Huang, T. Yao, Z. H. Sun, S. Q. Wei, X-ray absorption fine structure spectroscopy studies of thiol-capped copper nanoparticles, J. Phys.: Conference Series 430, (2013), 012033/1-012033/4.

[15] T. Kaito, H. Mitsumoto, S. Sugawara, K. Shinohara, H. Uehara, H. Ariga, S. Takakusagi, Y. Hatakeyama, K. Nishikawa, K. Asakura, K-Edge X-ray Absorption Fine Structure Analysis of Pt/Au Core-Shell Electrocatalyst: Evidence for Short Pt-Pt Distance, J. Phys. Chem. C 118, (2014), 8481-8490.

[16] T. Kondo, M. Okamura, K. Uosaki, Formation and electrochemical characteristics of multilayers of Au nanoclusters covered by mixed self-assembled monolayers of three kinds of alkanethiols with methyl, ferrocene, or carboxylate terminal group on Au(111) surface, Chem. Lett., (2001), 930-931.

[17] K. Uosaki, T. Kondo, M. Okamura, W. Song, Electron and ion transfer through multilayers of gold nanoclusters covered by self-assembled monolayers of alkylthiols with various functional groups, Faraday Discuss. 121, (2002), 373-389.

[18] W. Song, M. Okamura, T. Kondo, K. Uosaki, Electron and ion transport through multilayers of Au nanoclusters covered by self-assembled monolayers, J. Electroanal. Chem. 554, (2003), 385-393.

[19] W. Song, M. Okamura, T. Kondo, K. Uosaki, Construction and electrochemical characteristics of multilayer assemblies of Au nanoclusters protected by mixed self-assembled monolayers on tin-doped indium oxide, Phys. Chem. Chem. Phys. 5, (2003), 5279-5284.

[20] M. Okamura, T. Kondo, K. Uosaki, Electrochemical assembly and potential-dependent plasmon absorption of au nanoclusters covered with a 4-aminothiophenol self-assembled monolayer, J. Phys. Chem. B 109, (2005), 9897-9904.

[21] W. Song, M. Okamura, T. Kondo, K. Uosaki, Sequential layer-by-layer growth of Au nanoclusters protected by a mixed self-assembled monolayer with a polymer binding layer - Effects of pH and ionic strength of the polymer solution, J. Electroanal. Chem. 612, (2008), 105-111.

[22] M. Harada, N. Zanetakis, H. Noguchi, S. Takakusagi, K. Uosaki, Electrocatalytic activity for oxygen reduction of multilayer of Pd coated gold nanoclusters, Trans. Mater. Res. Soc. Jpn. 33, (2008), 1093-1096.

[23] M. Harada, H. Noguchi, N. Zanetakis, S. Takakusagi, W. Song, K. Uosaki, Construction of multilayers of bare and Pd modified gold nanoclusters and their electrocatalytic properties for oxygen reduction, Sci. Tech. Adv. Mater. 12, (2011), 044606.

[24] K. Uosaki, In situ real-time monitoring of geometric, electronic, and molecular structures at solid/liquid interfaces, Jpn. J. Appl. Phys. 54, (2015), 030102/1-030102/14.

[25] M. Brust, M. Walker, D. Bethell, D. J. Schiffrin, R. Whyman, Synthesis of Thiol-Derivatized Gold Nanoparticles in a Two-Phase Liquid-Liquid System, J. Chem. Soc., Chem. Commun., (1994), 801-802.

[26] M. J. Hostetler, A. C. Templeton, R. W. Murray, Dynamics of place-exchange reactions on monolayer-protected gold cluster molecules, Langmuir 15, (1999), 3782-3789.

[27] A. C. Templeton, F. P. Zamborini, W. P. Wuelfing, R. W. Murray, Controlled and reversible formation of nanoparticle aggregates and films using Cu^{2+}-carboxylate chemistry, Langmuir 16, (2000), 6682-6688.

[28] F. P. Zamborini, J. F. Hicks, R. W. Murray, Quantized double layer charging of nanoparticle films assembled using carboxylate/(Cu^{2+} or Zn^{2+})/carboxylate bridges, J. Am. Chem. Soc. 122, (2000), 4514-4515.

[29] D. I. Gittins, D. Bethell, R. J. Nichols, D. J. Schiffrin, Redox-connected multilayers of discrete gold particles: A novel electroactive nanomaterial, Adv. Mater. 11, (1999), 737-740.

[30] S. W. Chen, R. W. Murray, S. W. Feldberg, Quantized capacitance charging of monolayer-protected Au clusters, J. Phys. Chem. B 102, (1998), 9898-9907.

[31] R. Blonder, L. Sheeney, I. Willner, Three-dimensional redox-active layered composites of Au-Au, Ag-Ag and Au-Ag colloids, Chem. Commun., (1998), 1393-1394.

[32] S. Ye, A. Yashiro, Y. Sato, K. Uosaki, Electrochemical in situ FT-IRRAS studies of a self-assembled monolayer of 2-(11-mercaptoundecyl) hydroquinone, J. Chem. Soc., Faraday Trans. 92, (1996), 3813-3821.

[33] Y. Sato, S. Ye, T. Haba, K. Uosaki, Potential dependent orientation and oxidative decomposition of mercaptoalkanenitrile monolayers on gold. An in situ Fourier transform infrared spectroscopy study, Langmuir 12, (1996), 2726-2736.

[34] S. Ye, T. Haba, Y. Sato, K. Shimazu, K. Uosaki, Coverage dependent behavior of redox reaction induced structure change and mass transport at an 11-ferrocenyl-1-undecanethiol self-assembled monolayer on a gold electrode studied by an in situ IRRAS-EQCM combined system, Phys. Chem. Chem. Phys. 1, (1999), 3653-3659.

[35] T. d. F. Paulo, H. D. Abruña, I. C. N. Diógenes, Thermodynamic, Kinetic, Surface pK_a, and Structural Aspects of Self-Assembled Monolayers of Thio Compounds on Gold, Langmuir 28, (2012), 17825-17831.

[36] D. N. Batchelder, R. O. Simmons, X-Ray Lattice Constants of Crystals by a Rotating-Camera Method: Al, Ar, Au, CaF_2, Cu, Ge, Ne, Si, J. Appl. Phys. 36, (1965), 2864-2868.

[37] R. R. Preston, Quantitative Size-Factors for Gold-Manganese Solid Solutions, J. Mater. Sci. 1, (1966), 309-310.

[38] S. V. Nagender, C. R. Houska, X-Ray Determinations of Debye Temperatures and Thermal Expansions for Pd-Ag-Au System, J. Appl. Phys. 42, (1971), 4971-4975.

[39] R. Roberge, G. M. Leak, Study of Iron in Gold-Iron Alloys, Phys. Status Solidi A 19, (1973), 695-705.

[40] W. Slusark Jr, B. Lalevic, Fuschill.N, Structure and Electrical Conductivity of Cosputtered Gold-Chromium Alloy Films, J. Appl. Phys. 44, (1973), 2891-2892.

[41] A. L. Patterson, The determination of the size and shape of Crystal particles by x-rays, Phys. Rev. 49, (1936), 884.

[42] A. L. Patterson, The diffraction of x-rays by small crystalline particles, Phys. Rev. 56, (1936), 972-977.

[43] A. L. Patterson, The scherrer formula for x-ray particle-size determination, Phys. Rev. 56, (1939), 978-982.

[44] M. Cernohorsky, The Ratio Method for Absolute Measurements of Lattice Parameters with Cylindrical Cameras, Acta Crystallogr. 13, (1960), 823-826.

[45] K. E. Willis, An Explicit Expression for Lattice Parameters of Cubic Crystals for Ratio Method, Acta Crystallogr. 14, (1961), 1090-1091.

[46] R. H. Bragg, C. M. Packer, Effect of Absorption and Incoherent Scattering on X-Ray Line Profiles, Rev. Sci. Instrum. 34, (1963), 1202-1207.

[47] K. Page, T. Proffen, H. Terrones, M. Terrones, L. Lee, Y. Yang, S. Stemmer, R. Seshadri, A. K. Cheetham, Direct observation of the structure of gold nanoparticles by total scattering powder neutron diffraction, Chem. Phys. Lett. 393, (2004), 385-388.

[48] J. Harada, S. Yao, A. Ichimiya, X-Ray-Diffraction Study of Fine Gold Particles Prepared by Gas Evaporation Technique .1. General Feature, J. Phys. Soc. Jpn. 48, (1980), 1625-1630.

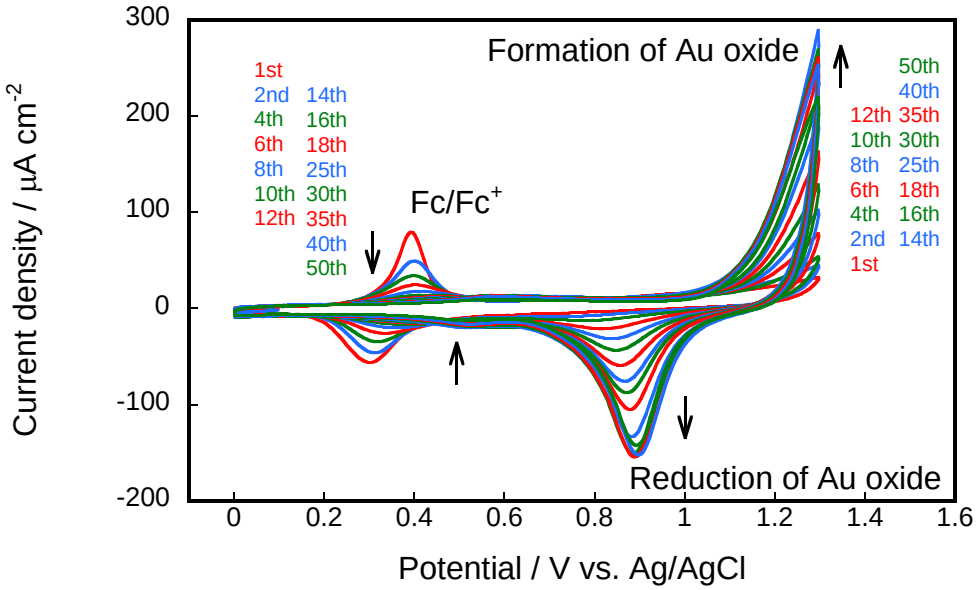

Fig. 1 T. Kondo et al.

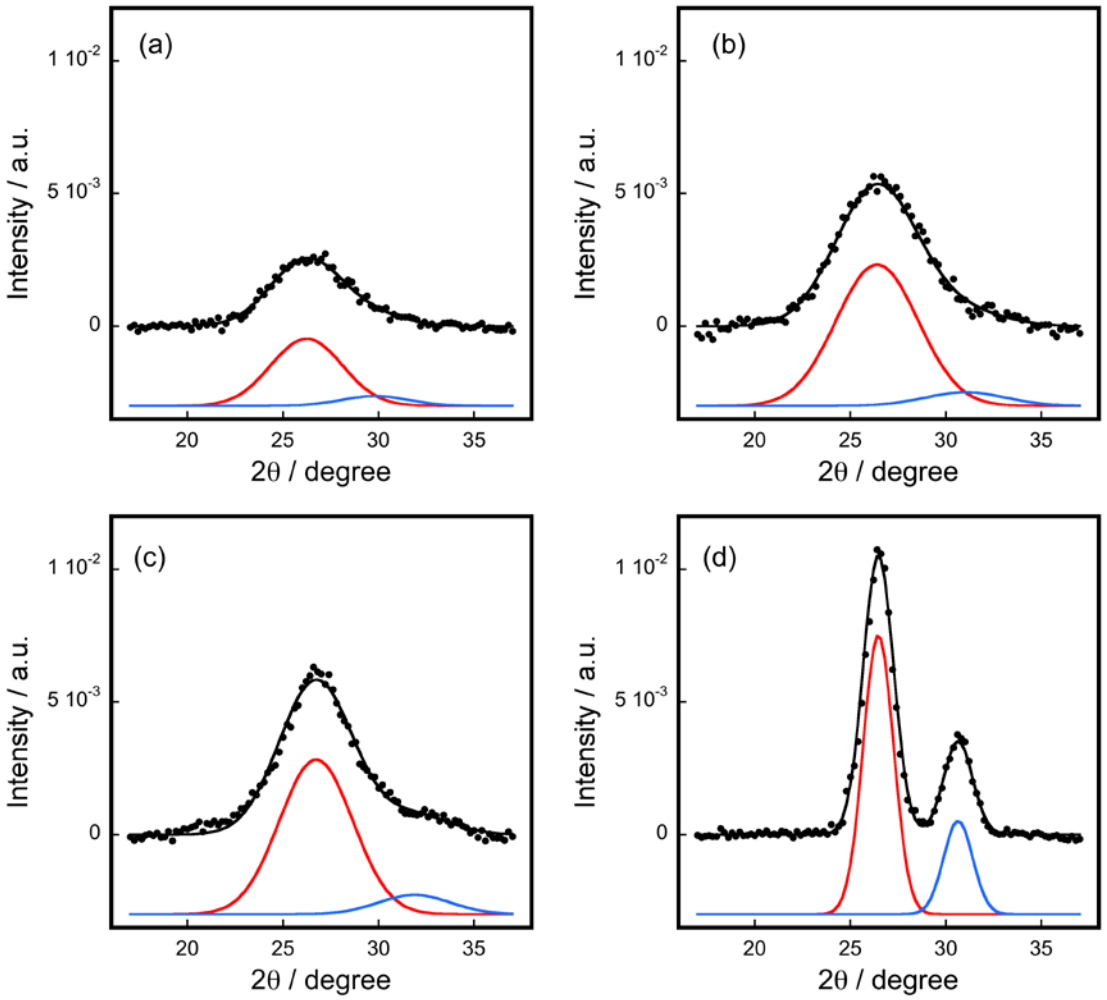

Fig. 2 T. Kondo et al.

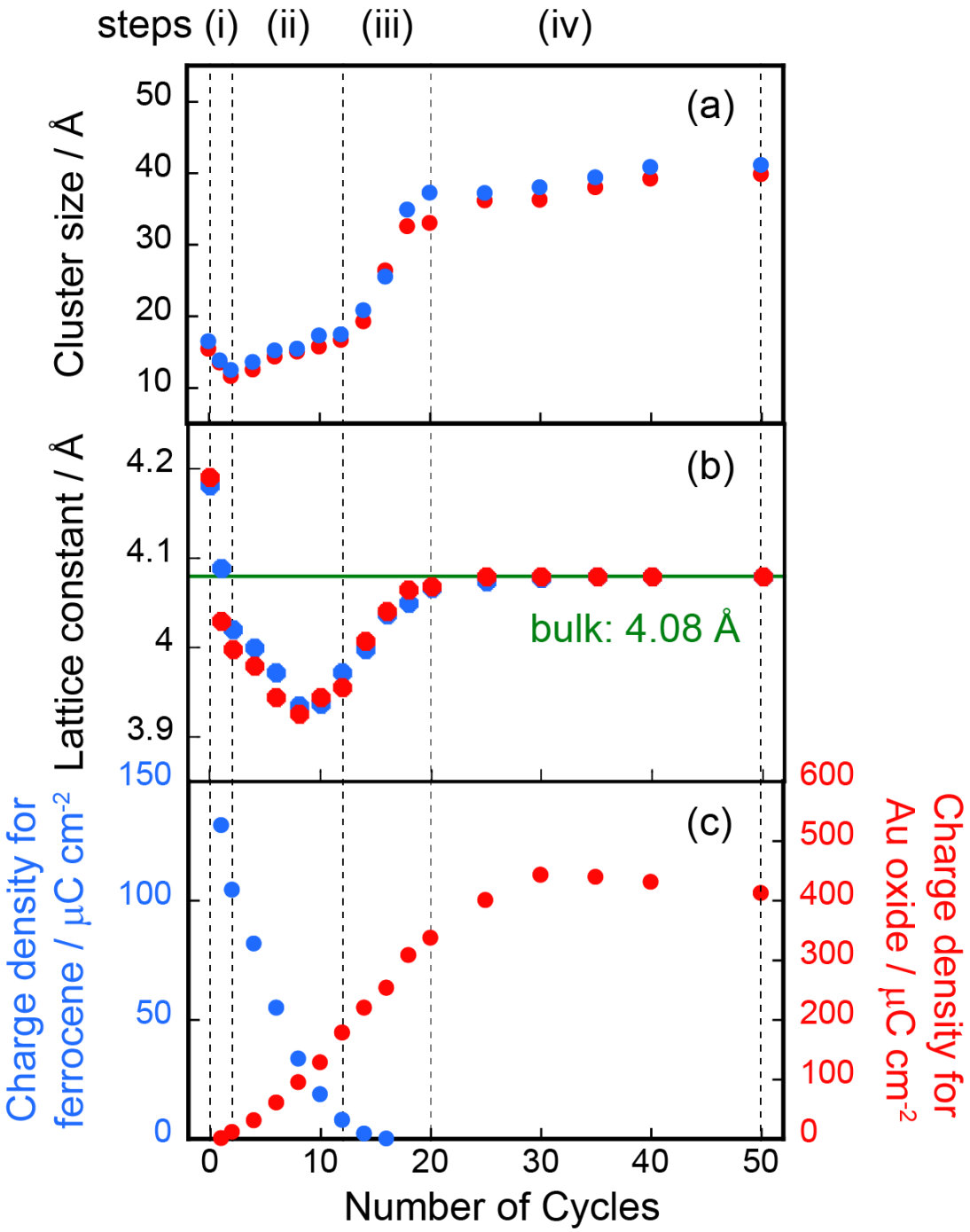

Fig. 3 T. Kondo et al.